

Cross-section measurement of the $^{18}\text{F}(\alpha, p)^{21}\text{Ne}$ reaction and possible implication for neutron production in explosive helium burning

H. Y. Lee,^{*} M. Couder, A. Couture,[†] S. Falahat,[‡] J. Görres, L. Lamm, P. J. LeBlanc, S. O'Brien, A. Palumbo, E. Stech, E. Strandberg, W. Tan, C. Ugalde,[§] and M. Wiescher

Department of Physics and The Joint Institute for Nuclear Physics, University of Notre Dame, Notre Dame, Indiana 46556, USA

(Received 9 June 2009; published 25 August 2009)

At the high temperature and density conditions of hot or explosive helium burning, the $^{18}\text{F}(\alpha, p)^{21}\text{Ne}$ reaction may compete successfully with the $^{18}\text{F}(\beta^+ \nu)$ decay. This suggests $^{21}\text{Ne}(\alpha, n)$ as an alternative neutron source in the r -process. We have determined the total cross section of the $^{18}\text{F}(\alpha, p)^{21}\text{Ne}$ reaction by studying the time-reverse reaction $^{21}\text{Ne}(p, \alpha)^{18}\text{F}$. Using the activation technique, the total reaction yield was measured in the proton beam energy range of 2.3–4.0 MeV, which corresponds to energies of 0.5–2.1 MeV in the $^{18}\text{F} + \alpha$ system. The resulting yield curve was analyzed in terms of the thick target formalism and the R -matrix theory. The reaction rate was deduced experimentally for the first time for the temperature of $0.1 < T_9 < 1$. The experimental reaction rate was compared with Hauser-Feshbach predictions. The astrophysical implications of the new rate are discussed.

DOI: [10.1103/PhysRevC.80.025805](https://doi.org/10.1103/PhysRevC.80.025805)

PACS number(s): 26.30.Hj, 24.30.-v, 24.60.Dr

I. INTRODUCTION

The astrophysical site of the r -process has been a long-standing question in nuclear astrophysics. One of the initial suggestions was the explosive helium burning in the shock-front of a type II supernova with high neutron flux being produced by the $^{21}\text{Ne}(\alpha, n)^{24}\text{Mg}$ reaction [1,2]. Isotopic anomalies in meteoritic materials [3], the results of detailed simulations for low mass elements ($12 \leq A \leq 22$) with different temperature-density profiles [4], and the propagation of the explosion shock wave of a supernova [5] suggested the possibility of such an r -process site [6]. It was shown [7] that an r -process can work at low densities ($\rho \lesssim 10^5 \text{ g/cm}^3$) and temperatures ($T_9 \approx 1$ –2), provided that some heavy seed nuclei are present in α -rich regions and that the nuclear time scales are shorter than the hydrodynamical time scale. This scenario could not be verified, however, because the neutron flux from $^{21}\text{Ne}(\alpha, n)$ was not sufficient to replicate the observed r -process abundance distribution [8].

Recent observations of ultra-metal-poor stars [9–11], however, have revived this scenario as a possible site for the weak r -process ($Z < 65$) [12]. Alternative nucleosynthesis paths have been considered for the shock-front-induced rapid increase of temperature and density in the helium-rich shell. The $^{14}\text{N}(\alpha, \gamma)^{18}\text{F}$ -induced $^{18}\text{F}(\alpha, p)$ reaction branch is strongly temperature dependent; the increase in temperature enhances the reaction rate, making it substantially faster than the $^{18}\text{F} \beta^+$ decay ($T_{1/2} = 109.77 \text{ min}$). Hauser-Feshbach estimates of the $^{18}\text{F}(\alpha, p)$ reaction rate suggest that this branch opens at

temperatures $T_9 > 0.4$, feeding the $^{21}\text{Ne}(\alpha, n)$ neutron source. Figure 1 illustrates the possible nuclear reaction paths around ^{18}F at different stellar temperature conditions.

While this scenario depends strongly on the available ^{14}N abundance from preceding CNO burning, it also is critical to determine an accurate reaction rate of $^{18}\text{F}(\alpha, p)^{21}\text{Ne}$. The currently used reaction rate for nucleosynthesis simulations is based on theoretical predictions using the Hauser-Feshbach formula. The Hauser-Feshbach predictions for sd -shell nuclei are not necessarily reliable because of the limited level densities in the compound nuclear system and therefore need to be tested experimentally.

A direct measurement of the $^{18}\text{F}(\alpha, p)^{21}\text{Ne}$ reaction is difficult because it requires the development of intense ^{18}F radioactive beams. The first test measurement at the radioactive beam facility, the Cyclotron Research Center of the Université Catholique de Louvain in Belgium, gave promising results but demonstrated the need for an improved target-detector array with better Q -value resolution [13]. An alternative approach is to study the time-reversed reaction $^{21}\text{Ne}(p, \alpha)^{18}\text{F}$ ($Q = -1.741 \text{ MeV}$). Such a measurement was attempted by Giesen [14] at the Dynamitron Tandem Laboratory (DTL) of Ruhr Universität Bochum in Germany. Giesen employed two different methods to determine the reaction cross section at energies between 2.5 and 4.6 MeV using the Bochum gas target [15]. Above 3 MeV proton energy the α_0 and α_1 reaction products were measured directly by using a silicon surface barrier detector. For lower energies, the activation method was employed. The reaction product ^{18}F was collected in an extended gas cell and the 511 keV annihilation activity was detected using a pair of NaI detectors in an off-line counting station. The activation data could cover the energy range of $2.3 \text{ MeV} < E_{\text{c.m.}} < 3.6 \text{ MeV}$, overlapping the range of the α -spectroscopy measurement. At energies below 3 MeV, the activation data deviated by up to 3 orders of magnitude from the Hauser-Feshbach prediction. This observed ^{18}F activity might have been caused by gas contamination of ^{18}O , which produces the same radioactive ^{18}F via a (p, n) reaction.

^{*}hylee@anl.gov; Present address: Argonne National Laboratory, Argonne, IL 60439, USA.

[†]Present address: Los Alamos National Laboratory, Los Alamos, NM 87545, USA.

[‡]Also: Max-Planck-Institut für Chemie, Geochemie, Joh.-J.-Becher-Weg 27, 55128 Mainz, Germany.

[§]Present address: Argonne National Laboratory, Argonne, IL 60439, USA.

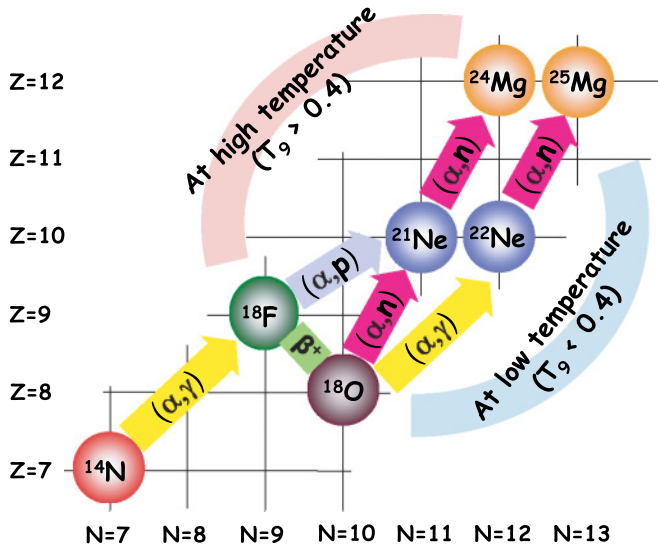


FIG. 1. (Color online) Nuclear reaction network of ^{18}F in a He-rich environment. The upper band shows a favored $^{18}\text{F}(\alpha, p)$ reaction when $T_9 > 0.4$ and the lower band indicates the dominant $^{18}\text{F}(\beta^+)$ decay when $T_9 < 0.4$.

In the present article we describe the remeasurement of the time-reversed reaction $^{21}\text{Ne}(p, \alpha)^{18}\text{F}$ at low energies, using a ^{21}Ne implanted target to avoid ^{18}O contamination in the gas target. The experimental setup is discussed in Sec. II and the results of the cross-section measurement are compared with the Hauser-Feshbach calculation in Sec. III. The reaction rate is derived and its impact on extra neutron production and r -process nucleosynthesis is discussed in the framework of nuclear reaction network simulations in Sec. IV. The conclusion and outlook are summarized in Sec. V.

II. EXPERIMENTAL SETUP

The experiments were made at the Nuclear Science Laboratory (NSL) of the University of Notre Dame. The measurement of the time-reversed reaction of $^{21}\text{Ne}(p, \alpha)^{18}\text{F}$ was performed at proton energies of 2.3–3.3 and 3.0–4.0 MeV using the KN Van de Graaff accelerator and the FN tandem accelerator, respectively. Implanted ^{21}Ne targets were irradiated with protons of different energies for two half-lives of ^{18}F , and then the 511 keV annihilation activity was counted off-line using the array of two clover HPGe-detectors in coincidence mode.

A major improvement from previous measurements was the reduction in the beam-induced background by the use of implanted ^{21}Ne targets instead of a ^{21}Ne gas target. Details of the target production and tests can be found in a separate article (Ref. [16], and references therein) and only the relevant parts are summarized here. Each implantation was performed at the 500 keV Cockcroft-Walton accelerator at the DTL of the Ruhr-Universität Bochum. The implantation was performed at two energies, 150 and 400 keV, to maximize the number of implanted ions and to achieve a uniform depth profile with a flat plateau at saturation. It was important to minimize

oxygen contamination of the backing material because this would generate beam-induced background from the reactions $^{18}\text{O}(p, n)^{18}\text{F}$ [17] and $^{17}\text{O}(p, \gamma)^{18}\text{F}$ [18,19]. These oxygen reactions produce ^{18}F , which is the desired reaction signature. There is no way to differentiate between ^{18}F produced from oxygen and that from Ne in the activation. This was achieved by using gold-plated copper (Cu/Au) backings that were cleaned and baked prior to activation. All the steps were tested to assure that no oxygen was added, that Ne migration was minimized, and that no etching of the target during chemical cleaning and baking procedures had occurred. Despite these preparations small trace amounts of oxygen remained in the Cu/Au backing. To correct for the amount of ^{18}F background activity, each measurement was performed with a ^{21}Ne -implanted target and a blank Cu/Au target that had been prepared in the same manner, except implantation.

The ^{21}Ne -implanted targets were water cooled during activation; a liquid nitrogen cold trap was mounted in front of the target to avoid carbon buildup. Narrow Resonance Analysis (NRA) and Deuteron-Induced γ -ray Emission (DIGE) methods were used to measure the target profile and to determine the absolute number of implanted ^{21}Ne ions and the amount of oxygen left on each target. This information was used to derive the background activity resulting from the remaining $^{17,18}\text{O}$ impurities. Because of the high beam intensity of 2–40 μA during activation, the target profiles were rescanned after accumulating different amounts of charge and a deterioration rate of $\sim 2\%$ per 1 C of protons was observed. The variation of beam current on a target was monitored and recorded to correct for the realistic irradiation rate as a function of time.

The off-line counting system has been optimized for measuring the two 511 keV γ -annihilation radiation events in coincidence. Two clover detectors [20], consisting of four individual HPGe crystals, were aligned face-to-face providing a nearly 4π detection arrangement. The activated target was inserted between the clover detectors. The thickness of the target holder, PVC, was specifically chosen to stop β^+ particles so that they annihilate within the 5-mm gap in between the detectors. The detector counting arrangement was surrounded by one layer of lead bricks mounted at a distance of 4 cm from the Ge crystals. A 1.25-cm-thick brass plate was attached on the inner wall of the top shield and 0.6-cm-thick copper plates were used to cover the remaining inner surfaces of the lead shield. The details of the setup can be found in Ref. [21]. With this passive shielding, the random coincidence rate for 511 keV γ rays from room background was measured to be about 0.6 counts/h.

Because the count rates during the measurement of a decay curve can vary between 5 and 1000 Hz per crystal, it was necessary to measure the system dead time as a function of time. For this purpose, a fixed frequency (100 Hz) from an oscillator was used to provide a time stamp and an external trigger to a pulse generator, feeding a 1 MeV equivalent pulse into the test input of one crystal of the clover detector. The ratio of detected pulses to the initially generated pulses was used to monitor the dead time of the detection system. A “good event” was recorded when both detectors triggered in coincidence. In addition to the hardware coincidence, a software coincidence with a narrow energy gate around 511 keV was also applied

to avoid the random coincidence with room background or the Compton scattered continuum.

III. DATA REDUCTION AND RESULTS

To determine the $^{21}\text{Ne}(p,\alpha)^{18}\text{F}$ cross section (σ) from the number of ^{18}F nuclei ($N(t)$) in the irradiated target, it is necessary to account for the number of ^{18}F nuclei decaying during irradiation. The change of the number of radioactive nuclei dN within a certain time window dt is expressed as

$$\begin{aligned} dN &= Pdt - \lambda N(t)dt \\ N(t) &= N_0 e^{-\lambda t} - \frac{P}{\lambda}(1 - e^{-\lambda t}), \end{aligned} \quad (1)$$

with $P = Y \times N_p/t$ being the production rate for a beam current $I = N_p/t$, where Y is the reaction yield corresponding to the number of (p,α) reactions per proton.

Because of fluctuations in the beam current on the target over time, Eq. (1) is solved numerically to sum the change of ^{18}F nuclei over each duration i , here used with 30 s to correct for the variation in charge collection. The change of ^{18}F nuclei at the i th duration, $dN_{^{18}\text{F}}|_i$, is the reaction yield produced with the average current I_i over 30 s (dt) and then subtracted for the decaying ^{18}F nuclei, which are accumulated up to the $(n-1)$ -th activation.

$$\begin{aligned} N_{^{18}\text{F}}|_n &= \sum_{i=1}^n dN_{^{18}\text{F}}|_i, \\ dN_{^{18}\text{F}}|_i &= Y \times (I_i dt - \lambda_{\beta^+} N_{^{18}\text{F}}|_{(n-1)} dt). \end{aligned} \quad (2)$$

Corrections were also required to account for ^{18}F decays occurring during the transport of the activated target from the activation chamber to the counting station as well as for residual activity from preceding activations to derive the total ^{18}F production.

A. Counting efficiency and decay curve fit

The counting efficiency of the two HPGe-clover detectors was determined using a ^{22}Na radioactive source. We derived the efficiency from the ratio between the detection of the two 511 keV annihilation radiation in coincidence with a 1274 keV γ ray and the single 1274 keV emission [22]. This method is independent of the absolute source strength and no summing corrections are necessary. The ^{22}Na calibration source had an extended area that approximately corresponded to the size of the beam spot on the target. The detection efficiency (η_{β^+}) for two coincident 511 keV γ -rays was determined to be $2.63 \pm 0.04\%$.

Other β^+ -decay components from background reactions were identified by analyzing the noncoincidence γ -ray spectra. As a result, the decay curve is fitted with fixed parameters for the known half-lives of a number of different components: (i) ^{13}N with a short half-life, caused by $^{12}\text{C}(p,\gamma)$ and $^{13}\text{C}(p,n)$ from the carbon deposited on the surface of the target; (ii) ^{18}F , the decay of interest; and (iii) ^{22}Na as an approximately constant background. The activity of ^{22}Na is produced by

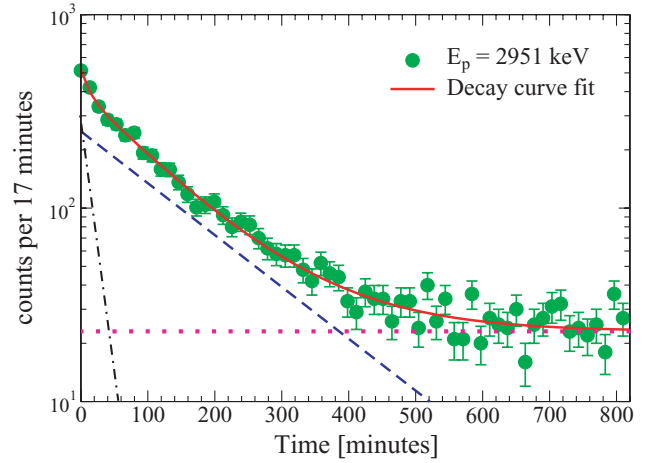


FIG. 2. (Color online) Fit of β^+ -decay curve with multi half-life components at $E_p = 2951$ keV. The dashed-dotted line is the decay curve of ^{13}N ($T_{1/2} \sim 10$ min), the dashed line is that of ^{18}F ($T_{1/2} \sim 110$ min), and the dotted line is that of ^{22}Na ($T_{1/2} \sim 2.6$ yr).

the $^{21}\text{Ne}(p,\gamma)$ background reaction. Because of this long lifetime of the last reaction, the overall constant background increased with multiple activations. As mentioned above there is (iv) the beam-induced ^{18}F background component originating mainly from the $^{18}\text{O}(p,n)^{18}\text{F}$ reaction on ^{18}O impurities in the Cu/Au target backing. For each energy step the measurements were performed with a ^{21}Ne -implanted target and a blank Cu/Au target. The ^{18}F background activity detected in a blank target was subtracted from the ^{18}F activity measured from the implanted target. The ^{18}F background activity observed below the $^{18}\text{O}(p,n)$ reaction threshold ($E_p = 2.574$ MeV) was attributed to the reaction $^{17}\text{O}(p,\gamma)$ [18,19].

The initial abundance of the various radioactive components after the activation was obtained by fitting the decay curve to multiple exponentials using the nonlinear error-weighted least-squares technique [23]. The fits were performed using the Gaussian approximation (χ_G^2) [24] and the Poisson approximation (χ_P^2) [25], which is more appropriate in cases of low statistics with the maximum likelihood method [26]. In our case both approaches gave similar results. Therefore, the Gaussian distribution was finally used as a consistent fit in the multicomponent decay curve analysis, as shown in Fig. 2.

B. Excitation curve of $^{21}\text{Ne}(p,\alpha)^{18}\text{F}$

The excitation curve of the reaction yield as a function of beam energy is shown in Fig. 3. The data points were measured in 30 keV energy steps. Because the ^{21}Ne targets are rather thick ($\xi \sim 25$ keV at $E_p \sim 3$ MeV), the measured yield from the present activation is derived as a “thick target yield” [27], possibly integrating the reaction cross section over several resonances. To compare this thick target yield with the previous results, we normalize it to the number of ^{21}Ne target nuclei per cm^2 , N_t , using Eq. (1): $Y_{\text{norm}} = Y/N_t$. This normalized yield would correspond to the cross section if the latter would be constant over the target thickness (thin target

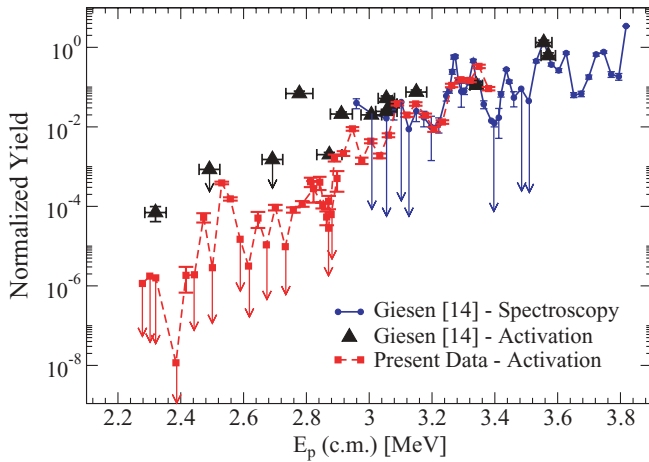


FIG. 3. (Color online) The normalized reaction yield for $^{21}\text{Ne}(p,\alpha)^{18}\text{F}$ as a function of energy in comparison with previous results. The vertical error bars in the present data represent the statistical uncertainties in the ^{18}F activity. Arrows indicate upper limits.

yield). The overall error budget for the normalized yield is shown in Table I.

Figure 3 shows good agreement between the previous spectroscopy data [14] and the present activation data in the region of overlap between 3.0 and 3.4 MeV. The previously obtained activation data at $E_p < 3$ MeV suggest higher yields compared to the present activation results. This is due to insufficient corrections for the ^{18}O contamination in the ^{21}Ne gas cell in the setup used in the Bochum experiment. The present data below 2.43 MeV provide only upper limits because of the decreasing reaction yield and the increase in accumulated ^{22}Na activity in the targets with repeated use. This upper limit is two orders of magnitude smaller than the value reported from the previous experiment [14]. In all, over six orders of magnitude in normalized yield were covered in this work.

We have calculated the Hauser-Feshbach cross section for $^{21}\text{Ne}(p,\alpha)^{18}\text{F}$ using the code SMOKER [29]. The yield was

TABLE I. Relative errors in the yield determination.

	Initial abundance	η_{β^+}	$\lambda_{^{18}\text{F}}$	N_t	N_p
Relative error (%)	0.1 ~ 40	1.4	0.05 [28]	~9	~3

derived directly from the calculated cross section ($\sigma_{\text{cal.}}$) using the approximation

$$Y_{\text{cal.}}(E) = \frac{1}{\varepsilon(E)} \int_{E-\xi}^E \sigma_{\text{cal.}}(E) dE. \quad (3)$$

As shown in the left panel in Fig. 4, overall the experimental data compare well with the Hauser-Feshbach prediction (dashed line). However, the prediction at lower energies is considerably lower than the experimental yield data, which are characterized by pronounced resonance structures.

Complementary to the Hauser-Feshbach statistical model approach, we therefore performed a more detailed resonance analysis using the single-channel Breit-Wigner formalism [30] as well as the multichannel R -matrix formalism [31] to extract information about the observed single-resonance structures. The Breit-Wigner formalism was used to determine directly the resonance strength $\omega\gamma$ from the thick target yield on resonance.

$$\omega\gamma = \frac{m_p}{(m_p + m_t)} \frac{2\varepsilon}{\lambda^2} Y_R, \quad (4)$$

with m_p (m_t) being the mass of the projectile (target), ε the stopping power, and λ the center-of-mass De Broglie wavelength at resonance energy. Deduced resonance strengths are used for determining the reaction rates in Sec. IV.

This approach neglects possible resonance interference effects in the cross section description. For a more extensive analysis of all reaction components we used the R -matrix code AZURE [32] to model the cross-section excitation curve. Unfortunately, there is very limited information available about the level structure of the compound nucleus ^{22}Na in the excitation range we measured, above the α threshold. For this reason the R -matrix fit of the total reaction yield

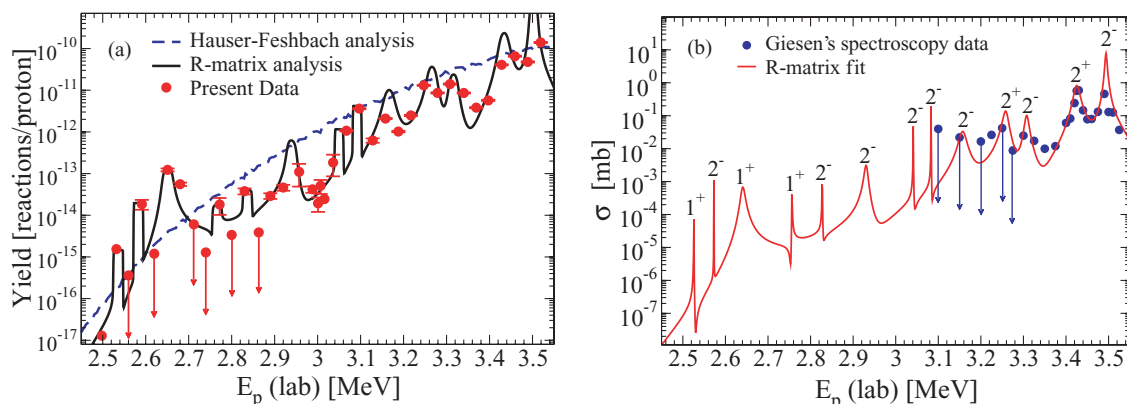


FIG. 4. (Color online) Panel (a) shows comparison between the present experimental yields and the yield prediction from Hauser-Feshbach calculations (dashed line) and the calculations based on an R -matrix fit to the data (solid line). Panel (b) shows the R -matrix cross section, which is obtained by fitting to the previous spectroscopy data [14] as described in the text.

cannot provide a unique assignment of level parameters, such as resonance energy, J^π values, and partial widths for most of the states observed in the current energy range. For resonances with unknown spins and parities we adopted the lowest possible ℓ values. First, the calculated R -matrix cross section, shown in the right panel in Fig. 4, was obtained by fitting the available spectroscopic information at $E_p > 3.1$ MeV from Giesen's measurements. Then, for each energy step it was integrated over the actual target thickness using Eq. (4) to compare the overall fit with our measured yield. The stopping cross section, $\varepsilon(E)$, is approximately constant over the current target thickness. The calculated R -matrix yield (solid line) was iterated by varying the partial widths and the sign of interference of each resonance until it was consistent with the data. The details of the fitting procedure are discussed in Ref. [33]. Considering the limited spectroscopic information available, this represents only an attempt to estimate the reaction rate, which is discussed in the following section.

IV. REACTION RATES AND ASTROPHYSICAL IMPLICATIONS

A. Determination of reaction rates

The reaction rate based on the present data was calculated using two different methods. In the first approach the rate for $^{21}\text{Ne}(p,\alpha)^{18}\text{F}$ was calculated by integrating the experimental cross section $\sigma(E)$ (see Fig. 4) over the Maxwell-Boltzmann distribution of a stellar gas at temperature T ,

$$\langle\sigma v\rangle = \left(\frac{8}{\pi\mu}\right)^{1/2} (kT)^{-3/2} \int \sigma(E)E \exp\left(-\frac{E}{kT}\right) dE. \quad (5)$$

Here E is the energy of the particles in the center of mass system, N_A Avogadro's number, k Boltzmann's constant, and μ the reduced mass. We used the cross section obtained from the multichannel R -matrix analysis described in Sec. III B.

The second method for determining the reaction rate was based on the measurement of the on-resonance yield (Y_R). Assuming thick target yield conditions, the on-resonance yield corresponds directly to the resonance strength, $\omega\gamma$. Within that approach the reaction rate for $^{21}\text{Ne}(p,\alpha)^{18}\text{F}$ is obtained by summing over each individual resonance i as

$$\langle\sigma v\rangle = \left(\frac{2\pi}{\mu kT}\right)^{3/2} \hbar^2 \sum_i (\omega\gamma)_i \exp\left(-\frac{E_i}{kT}\right). \quad (6)$$

The reaction rate for the inverse $^{18}\text{F}(\alpha,p)^{21}\text{Ne}$ reaction was subsequently derived using the detailed balanced theorem for $1 + 2 \rightarrow 3 + 4$ as

$$\langle\sigma v\rangle_{12} = \langle\sigma v\rangle_{34} \frac{(2J_3 + 1)(2J_4 + 1)}{(2J_1 + 1)(2J_2 + 1)} \left(\frac{\mu_{12}}{\mu_{34}}\right)^{-3/2} \exp\left(\frac{Q}{kT}\right). \quad (7)$$

The experimental rates are compared with a number of Hauser-Feshbach predictions based on the code SMOKER [29] and the modified and improved versions MOST [34],

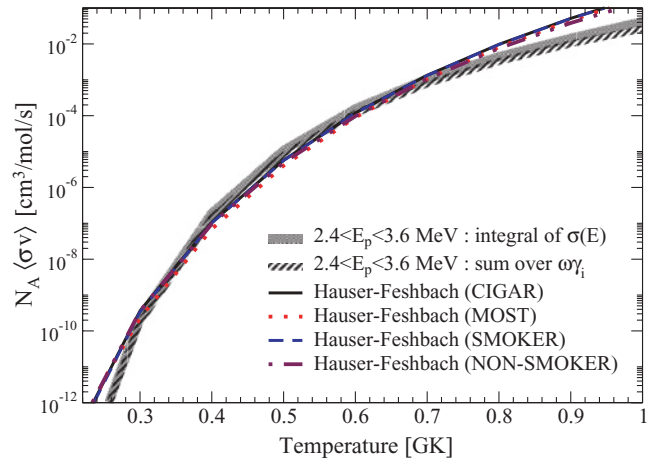


FIG. 5. (Color online) Comparison of the $^{18}\text{F}(\alpha,p)^{21}\text{Ne}$ reaction rates derived by two different methods using the present data: the shaded line is the integration of analytical cross sections obtained from the R -matrix fit, and the diagonal-stripe line is the sum over the individual resonance strengths deduced using the thick target yield. The Hauser-Feshbach predictions are shown together; see text for details.

NON-SMOKER [35], and CIGAR [36]. All predictions are in excellent agreement as demonstrated in Fig. 5. The reaction rate obtained by integrating over the cross section (dashed line) agrees well with the rate based on the thick target yield approximation (diagonal-stripped line). The established experimental rates are slightly higher (by about a factor of two) than the Hauser-Feshbach predictions at temperatures $0.3 < T_9 < 0.6$. However, at low temperatures $T_9 < 0.3$ and at high temperatures $T_9 > 0.6$ the Hauser-Feshbach rates are substantially higher than the experimental rates. Because the proton energies $2.4 < E_p(\text{laboratory}) < 3.6$ MeV in the current work correspond to the effective temperature range $0.4 < T_9 < 1.1$, we have estimated the contribution of the rate from the currently unmeasured resonances below 2.4 MeV. For the unknown resonance strengths, we used the calculated single-particle widths with spectroscopic factors between 0.001 and 0.01 to obtain the partial widths (Γ_p and Γ_α). Adding this estimate did not change the rate deduced from the data, so we could exclude the possible influence of unmeasured resonances in the temperature range of our interest.

Based on the present analysis of the experimental data we conclude that on average the Hauser-Feshbach approach overestimates the rate at temperatures where it is dominated by closely spaced resonances. For this reason we normalized the Hauser-Feshbach rate to the experimental rate by scaling it with a factor of 2.3, which represents the average ratio of the two rates at $0.3 < T_9 < 0.6$. The recommended rate was adopted from the experimental rate for $0.3 < T_9 < 0.6$ and for all other temperatures from the renormalized Hauser-Feshbach rate and is shown in Fig. 6. This rate carries a large uncertainty; the upper limit of the rate is based on using the upper limit of the measured yield at around 2.4 MeV for calculating the reaction rate. The lower limit of the reaction rate corresponds to the lower limit of the measured yields without taking possible higher energy or lower energy resonances into account. The

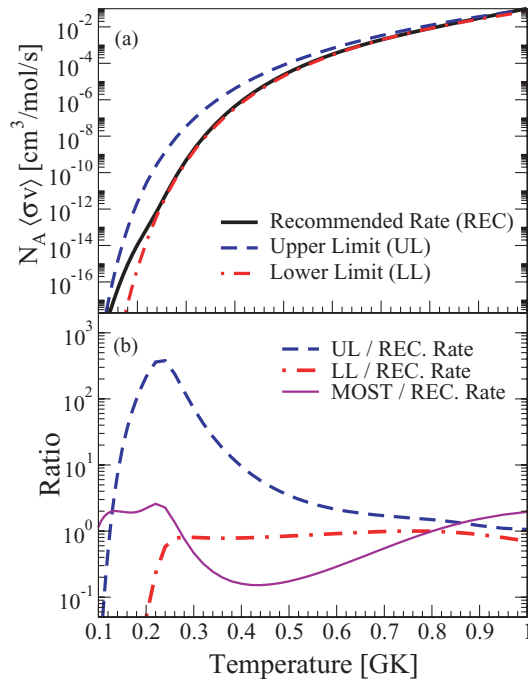


FIG. 6. (Color online) (a) The recommended rate for the $^{18}\text{F}(\alpha, p)^{21}\text{Ne}$ reaction with the upper and the lower limits. In panel (b), both limits and theoretical Hauser-Feshbach calculations, MOST, are normalized to the recommended rate.

recommended reaction rate is also listed in Table II as well as the upper and lower limits. For comparison also listed are the predicted Hauser-Feshbach rates using the code MOST [34].

B. Network calculation for *r*-process

To investigate the impact of the current experimental rate for the reaction $^{18}\text{F}(\alpha, p)^{21}\text{Ne}$, the shock-front-driven explosive nucleosynthesis and the associated neutron production in the helium burning shell of the pre-supernova star were simulated for a $15M_{\odot}$ star [37]. The hydrodynamic multizone supernova explosion model [38] generates the temperature and density profile for the time the shock reaches the He-rich shell. Because the energy generation is driven by the shock, the nuclear energy is negligible and the nucleosynthesis network simulation can be performed in postprocessing mode. With the shock reaching the helium layer about 2 s after rebound, the temperature T_0 increases rapidly from 0.2 to 1.4 and declines slowly back to 0.25 in about 20 s. Similarly, the density increases from $\sim 700 \text{ g/cm}^3$ to $\sim 4000 \text{ g/cm}^3$ and declines exponentially. About 1200 isotopes are used to simulate the associated nucleosynthesis. In particular, we explore the abundance evolution of F, Ne, and Mg nuclei to look for signatures for a possible alternative neutron source.

Figure 7(a) presents the development of selected isotopic abundances for low mass nuclei during the 2 s the shock transverses the He shell. The figure indicates in particular ^{21}Ne (dash-dotted line), neutrons (dashed line), and ^{24}Mg (dotted line) abundances to monitor the impact of the recommended $^{18}\text{F}(\alpha, p)$ rate. Fig. 7(b) shows the abundances of ^{15}O , ^{18}F ,

TABLE II. Reaction rate ($\text{cm}^3/\text{mol/s}$) of $^{18}\text{F}(\alpha, p)^{21}\text{Ne}$.

Temp. (GK)	Recommended	Upper limit	Lower limit	MOST [34]
0.1	7.53×10^{-23}	3.29×10^{-25}	4.90×10^{-33}	1.79×10^{-22}
0.15	7.60×10^{-18}	1.32×10^{-16}	9.23×10^{-22}	1.81×10^{-17}
0.2	1.08×10^{-14}	2.33×10^{-12}	5.35×10^{-16}	2.57×10^{-14}
0.25	2.35×10^{-12}	7.64×10^{-10}	1.72×10^{-12}	4.46×10^{-12}
0.3	5.01×10^{-10}	3.49×10^{-8}	3.87×10^{-10}	2.27×10^{-10}
0.4	4.17×10^{-7}	4.10×10^{-6}	3.42×10^{-7}	6.95×10^{-8}
0.5	2.32×10^{-5}	7.96×10^{-5}	1.96×10^{-5}	4.05×10^{-6}
0.6	3.33×10^{-4}	6.63×10^{-4}	2.84×10^{-4}	8.96×10^{-5}
0.7	2.22×10^{-3}	3.35×10^{-3}	1.91×10^{-3}	1.06×10^{-3}
0.8	9.34×10^{-3}	1.21×10^{-2}	8.11×10^{-3}	8.12×10^{-3}
0.9	2.98×10^{-2}	3.52×10^{-2}	2.61×10^{-2}	4.53×10^{-2}
1	8.34×10^{-2}	8.97×10^{-2}	7.15×10^{-2}	1.98×10^{-1}

and ^{21}Ne using three different $^{18}\text{F}(\alpha, p)$ rates; the solid lines represent the abundances using the recommended rate, the dashed lines represent the Hauser Feshbach prediction, and the dash-dotted lines reflect the abundances without any $^{18}\text{F}(\alpha, p)$ rate. The ^{21}Ne abundance is insensitive to the choice of $^{18}\text{F}(\alpha, p)$ rate. This suggests that ^{21}Ne is primarily produced

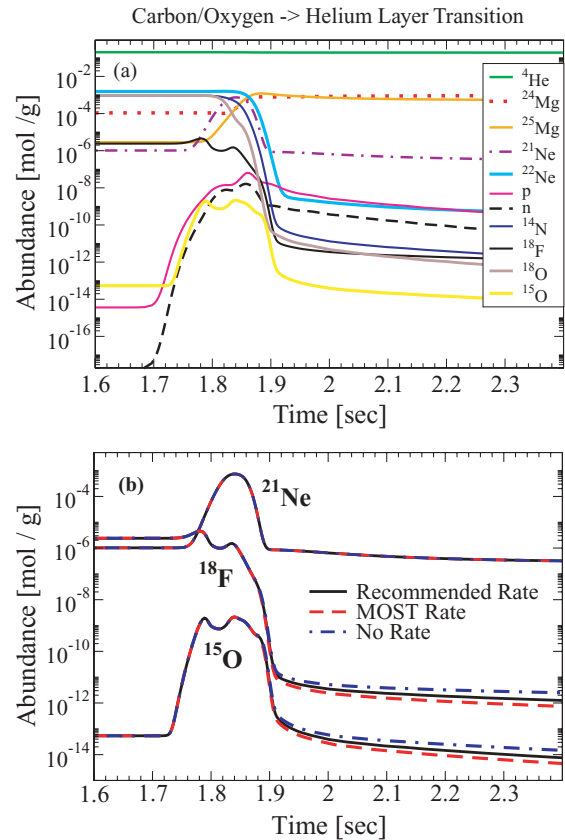


FIG. 7. (Color online) Evolution of elemental abundances in explosive He burning in the shock-front of a $15M_{\odot}$ core collapse supernova. The simulations are based on our recommended rate for $^{18}\text{F}(\alpha, p)^{21}\text{Ne}$ in Panel (a). Panel (b) compares isotopes of interest resulting from the different $^{18}\text{F}(\alpha, p)^{21}\text{Ne}$ rates.

by the $^{18}\text{F}(\beta\nu)^{18}\text{O}(\alpha, n)$ reaction sequence and by other, more complex, reaction sequences involving neutrons [39]. The production of ^{15}O depends on the $^{18}\text{F}(p, \alpha)$ reaction, which at higher temperatures $T_9 > 1$ becomes compatible with the $^{18}\text{F}(\alpha, p)^{21}\text{Ne}$ reaction [40].

V. SUMMARY AND CONCLUSION

The $^{18}\text{F}(\alpha, p)^{21}\text{Ne}$ reaction has been studied through the time-reversed $^{21}\text{Ne}(p, \alpha)^{18}\text{F}$ reaction process at proton energies from 2.3 to 4.0 MeV using activation techniques. The present cross-section measurement shows good agreement with the previous results of the α -spectroscopy by Giesen [14]. The reaction yield was analyzed within the framework of the thick target approximation and the multichannel R -matrix theory. Comparison between the measured yield and the calculated yield from R -matrix theory indicates prominent resonant structures. The lack of detailed level information above the α threshold in the compound nucleus ^{22}Na prevents a detailed analysis of the resonance contributions. The reaction rate was deduced using two different methods for the temperature range of interest; the direct integrating of the cross sections over a Maxwell-Boltzmann distribution and the summation of resonance strengths. The reaction rates derived by the two methods are in good agreement. The current data also agree within a factor of two with Hauser-Feshbach predictions in the temperature range $T_9 < 0.3$ and $T_9 > 0.6$. Larger differences in the data from the predictions observed for the intermediate temperature range reflect the impact of the measured individual resonances. The reaction rate was applied to simulate explosive helium burning in a supernova shock-front scenario. The results of the network calculations

do not show any significant impact of the reaction process. However, the enhanced reaction rate at the temperatures $0.3 < T_9 < 0.6$ affects the fluorine nucleosynthesis in AGB stars and Ne isotopic compositions of SiC grains [41]. The $^{18}\text{F}(\alpha, p)^{21}\text{Ne}$ reaction supplies extra protons to be captured on ^{18}O to facilitate the $^{18}\text{O}(p, \alpha)^{15}\text{N}(\alpha, \gamma)^{19}\text{F}$ chain. In particular, this study agrees remarkably with observations when the current upper limit of the $^{18}\text{F}(\alpha, p)^{21}\text{Ne}$ reaction rate is used. This suggests further experimental works at $E_p < 2.4$ MeV are necessary to narrow down the upper limit for the temperature range of the nucleosynthesis for AGB stars. Because the current upper limit is determined by the beam-induced background while counting the ^{18}F activity, another experiment could be the inverse kinematic study of the $p(^{21}\text{Ne}, \alpha)^{18}\text{F}$ reaction with the ^{21}Ne beam by detecting the α and the recoiling ^{18}F . Also further spectroscopic studies above the α threshold in ^{22}Na will help to reduce the uncertainty in reaction rates.

ACKNOWLEDGMENTS

The authors thank J. Kaiser, B. Mulder, and J. Lingle for their great assistance during the experiment. Special thanks to H.-W. Becker (Ruhr-Universität Bochum) for the hospitality and support during target implantations. The authors acknowledge A. Heger, T. Elliot, and H. Schatz for providing the input for pre-supernovae and helping network calculations. This work was supported by the National Science Foundation NSF Grant 0434844 and the Joint Institute for Nuclear Astrophysics JINA PHY02-16783. H.Y.L. acknowledges support from the US Department of Energy, Office of Nuclear Physics, under Contract DE-AC02-06CH11357.

-
- [1] J. B. Blake and D. N. Schramm, *Astrophys. J.* **209**, 846 (1976).
 - [2] W. Hillebrandt and F.-K. Thielemann, in *Proceedings of the Annual Meetings of the German Astronomical Society*, Basel (1977).
 - [3] F.-K. Thielemann, M. Arnould, and W. Hillebrand, *Astron. Astrophys.* **74**, 175 (1979).
 - [4] M. Arnould and W. Beelen, *Astron. Astrophys.* **33**, 215 (1974).
 - [5] S. A. Colgate, *Astrophys. J.* **187**, 321 (1974).
 - [6] J. W. Truran, J. J. Cowan, and A. G. W. Cameron, *Astrophys. J.* **222**, 63L (1978).
 - [7] W. Hillebrandt and F. K. Thielemann, *Astron. Astrophys.* **58**, 357 (1977).
 - [8] J. B. Blake, S. E. Woosley, T. A. Weaver, and D. N. Schramm, *Astrophys. J.* **248**, 315B (1981).
 - [9] J. W. Truran and J. J. Cowan, in *Proceedings of The 10th Workshop on Nuclear Astrophysics (2000)*, p. 64.
 - [10] A. G. W. Cameron, in *Proceedings of The Michigan R-Process Workshop (2002)*.
 - [11] J. J. Cowan and C. Sneden, in *Proceedings of The 12th Workshop on Nuclear Astrophysics (2004)*, p. 41.
 - [12] J. J. Cowan and C. Sneden, in *3-D Signatures in Stellar Explosions* (Cambridge University Press, Cambridge, UK, 2004), p. 255.
 - [13] H. Y. Lee, C. Angulo, H. W. Becker, E. Casarejos, M. Couder, A. Couture, B. Fulton, J. Görres, D. Groombridge, A. Laird, P. Leleux, E. Stech, E. Strandberg, W. Tan, C. Ugalde, and M. Wiescher, *PoS(NIC-IX)* **131**, 521 (2008).
 - [14] U. Giesen, Diploma thesis, Universität Münster, 1987.
 - [15] H. W. Becker, W. E. Kieser, C. Rolfs, H. P. Trautvetter, and M. Wiescher, *Z. Phys. A* **305**, 319 (1982).
 - [16] H. Y. Lee, J. Görres, E. Stech, E. Strandberg, M. Wiescher, and H.-W. Becker, *Nucl. Instrum. Methods B* (in press).
 - [17] J. K. Bair, *Phys. Rev. C* **8**, 120 (1973).
 - [18] J. C. Sens, S. M. Refaei, A. Ben Mohamed, and A. Pape, *Phys. Rev. C* **16**, 2129 (1977).
 - [19] C. Rolfs, *Nucl. Phys. A* **217**, 29 (1973).
 - [20] P. K. Joshi, H. C. Jain, A. S. Medhi, S. Chattopadhyay, S. Bhattacharya, and A. Goswami, *Nucl. Instrum. Methods A* **399**, 51 (1997).
 - [21] N. Özkan, G. Efe, R. T. Güray, A. Palumbo, J. Görres, H. Y. Lee, L. O. Lamm, W. Rapp, E. Stech, M. Wiescher, Gy. Gyürky, Zs. Fülöp, and E. Somorjai, *Phys. Rev. C* **75**, 025801 (2007).
 - [22] J. Görres, C. Arlandini, U. Giesen, M. Heil, F. Käppeler, H. Leiste, E. Stech, and M. Wiescher, *Phys. Rev. C* **62**, 055801 (2000).
 - [23] P. R. Bevington, *Data Reduction and Error Analysis for the Physical Science* (McGraw-Hill, New York, 1969).
 - [24] G. F. Grinyer *et al.*, *Phys. Rev. C* **71**, 044309 (2005).

- [25] S. Baker and R. D. Cousins, *Nucl. Instrum. Methods* **221**, 437 (1984).
- [26] K. E. Gregorich, *Nucl. Instrum. Methods A* **302**, 135 (1991).
- [27] W. A. Fowler, C. C. Lauritsen, and T. Lauritsen, *Rev. Mod. Phys.* **20**, 236 (1948).
- [28] National Nuclear Data Center, <http://www.nndc.bnl.gov>.
- [29] F. K. Thielemann, M. Arnould, and J. W. Truran, in *Advances in Nuclear Astrophysics*, edited by E. Vanghioni-Flam *et al.* (Editions Frontières, Paris, 1986), p. 525.
- [30] G. Breit, E. U. Condon, and R. D. Present, *Phys. Rev.* **50**, 825 (1936).
- [31] A. M. Lane and R. G. Thomas, *Rev. Mod. Phys.* **30**, 257 (1958).
- [32] R. Azuma, Multichannel *R*-matrix code (AZURE), <http://www.nd.edu/~azure>.
- [33] H. Y. Lee, Ph.D. thesis, University of Notre Dame, 2006.
- [34] M. Aikawa, M. Arnould, S. Goriely, A. Jorissen, and K. Takahashi, *Astron. Astrophys.* **441**, 1195 (2005).
- [35] T. Rauscher, F.-K. Thielemann, and K.-L. Kratz, *Phys. Rev. C* **56**, 1613 (1997).
- [36] R. Crowter, Diploma thesis, University of Surrey, 2008.
- [37] T. Elliot and H. Schatz, X-ray Burst Network Code: MSU (unpublished).
- [38] A. Heger, Multizone Supernova Explosion Code (unpublished, 2004).
- [39] M. Arnould and H. Nørgaard, *Astron. Astrophys.* **64**, 195 (1978).
- [40] M. Wiescher and K.-U. Kettner, *Astrophys. J.* **263**, 891 (1982).
- [41] A. I. Karakas, H. Y. Lee, M. Lugaro, J. Görres, and M. Wiescher, *Astrophys. J.* **676**, 1254 (2008).